Polymer Bulletin (2019) 76:2097–2111
https://doi.org/10.1007/s00289-018-2459-y

ORIGINAL PAPER

Effect of PEDOT:PSS content on structure and properties of PEDOT:PSS/poly(vinyl alcohol) composite fiber

Xin-yue Wang[1,2] · Gu-yu Feng[1,2] · Meng-juan Li[1,2] · Ming-qiao Ge[1,2]

Received: 18 October 2017 / Revised: 13 July 2018 / Accepted: 23 July 2018 / Published online: 17 August 2018

Abstract

In this study, effect of PEDOT:PSS content on structure and properties of poly(3,4-ethylenedioxythiophene):poly(styrenesulfonate) (PEDOT:PSS)/poly(vinyl alcohol) (PVA) composite conducting fiber was systematically investigated for the first time. PEDOT:PSS/PVA composite conducting fibers with various PEDOT:PSS loadings were successfully fabricated via wet-spinning technique. Correlation between PEDOT:PSS loading and performance of composite fibers was investigated by analyzing changes in chemical constitution, morphology, thermal property, conductivity, and tensile property of composite fibers. Formation of hydrogen bonding interactions was observed between PVA matrix and PEDOT:PSS conducting filler, and the interaction was enhanced with increasing PEDOT:PSS loading. As PEDOT:PSS loading increased in composite fiber, fiber conductivity increased monotonically, and surface morphology of composite fibers became regularly circular. Young's modulus and tensile strength of composite fibers also increased with increasing PEDOT:PSS loading, while elongation at break decreased. In addition, thermal stability of composite fibers improved with increasing PEDOT:PSS loading.

Keywords Conjugated polymer · PEDOT:PSS · Composite fiber · Conductivity · Hydrogen bonding interaction

✉ Ming-qiao Ge
ge_mingqiao@126.com

Xin-yue Wang
wangxinyue330@163.com

Gu-yu Feng
fengguyu890@163.com

Meng-juan Li
mjjn@jiangnan.edu.cn

[1] Key Laboratory of Science and Technology of Eco-Textiles, Ministry of Education, Jiangnan University, Wuxi 214122, China

[2] College of Textile and Clothing, Jiangnan University, Wuxi 214122, China

Introduction

Development of conducting polymer fibers based on conjugated polymers has played an important role in the realization of flexible electronic devices and smart electronic textiles [1]. They have been widely studied due to their inherent electrical conductivity, electrochromic property, [2] charge storage capabilities [3], and excellent processibility to be fabricated by wet-spinning technique. These properties provide for a wide range of utility in applications such as flexible display devices [2], energy-storage electrodes [4], and electrochemical actuators [5] which could be potentially integrated as flexible smart components of multifunctional textiles [3].

Various conjugated polymers have been successfully produced into fibers such as polyaniline, polypyrrole, and polythiophene. Polyaniline fiber stands out for its high conductivity and ability to be easily processed with relatively low cost [6, 7]. However, it needs an acid environment to retain high conductivity [8], and the presence of benzidine moieties in polymer chain might yield toxic and carcinogenic products during degradation [6, 9], which limited its development. Polypyrrole and polythiophene are more environmentally friendly and biocompatible, being suitable and potential for various utility of applications, though disadvantages of being insoluble and infusible made it difficult for bulk production. Therefore, researchers made unremitting efforts to develop various polythiophene derivatives to overcome these problems.

Poly(3,4-ethylenedioxythiophene):poly(styrenesulfonate) (PEDOT:PSS), as one of the most commercially successful polythiophene derivatives, featuring high conductivity, superior thermal and environmental stability, especially excellent processibility from aqueous dispersions, has been widely used in many fields [10, 11]. It has been successfully spun into microfibers from its aqueous solution by wet-spinning technique. PEDOT:PSS fibers are favored by many researchers due to their advantages over films. Okuzaki et al. [12] reported successful preparation of PEDOT:PSS fiber and improved fiber conductivity by EG dipping method. Jalili et al. [3] reported that continuous PEDOT:PSS fiber with high electrical conductivity was successfully fabricated with a simple one-step wet-spinning technique. Although PEDOT:PSS fibers have high conductivity, their poor mechanical property due to inherent stiffness and brittleness resulted from high modulus usually caused failure in weaving process. Thereby, it is intensively required that some other organic polymers such as polyvinyl alcohol (PVA), polyurethane (PU), and polyacrylonitrile (PAN) be blended with PEDOT:PSS to improve mechanical property of PEDOT:PSS fibers simultaneously to reduce preparation cost for broader applications.

As PVA is water soluble and the spinning process is relatively simple and environmentally friendly, we choose PVA to blend with PEDOT:PSS for preparing composite fiber that is expected to have good mechanical property. As far as I know, there has no article reported about study on the effect of PEDOT:PSS loading on structure and properties of PEDOT:PSS/PVA composite fibers.

Therefore, in this study, we systematically investigated for the first time the effect of PEDOT:PSS loading on structure and properties of PEDOT:PSS/PVA

composite fibers. We demonstrated an environmentally friendly method to prepare continuous PEDOT:PSS/PVA microfibers with good mechanical properties simultaneously ensuring relatively high conductivity by wet-spinning technique. This preparation process could be scaled up to industrial production. And then we systematically investigated the correlation between PEDOT:PSS loading and structure and properties of PEDOT:PSS/PVA composite fibers by analyzing changes in chemical structure, morphology, thermal property, electrical conductivity, and tensile property.

Experimental

Materials

PEDOT:PSS aqueous solution(Clevios P) was purchased from HC Starck, Inc. The 99.9% hydrolyzed PVA (DP = 3500) samples were provided by Kuraray Co. Ltd, Tokyo, Japan. Water used in the system was distilled water. All reagents used in the experiment were of analytically pure grade.

Preparation of composite spinning formulations

PVA was dissolved into distilled water to prepare PVA solution with a concentration of 100 mg mL^{-1}. PEDOT:PSS dispersions were mixed with PVA solution at various volume fractions to obtain composite spinning formulations with different PEDOT:PSS loadings which varied from 0 to 15 mg mL^{-1} (specific composite spinning formulations are shown in Table 1). Mixed spinning formulations were then homogenized at 3000 rpm (Wiggens WB3000-D) for 6 h at a constant temperature of 90 °C (IKA) to prepare homogeneous spinning formulations for subsequent wet-spinning process.

Preparation of composite fibers with various PEDOT:PSS loadings

Spinning formulations were injected into the syringe and then extruded into methyl alcohol coagulation bath through the needle (20 gauge) with a blunt tip. The

Table 1 PVA/PEDOT:PSS composite spinning formulations at different PEDOT:PSS contents

Sample No.	PVA (mg mL^{-1})	PEDOT:PSS (mg mL^{-1})	PEDOT:PSS content (wt%)
1	100	0	0
2	100	2	1.96
3	100	3	2.91
4	100	5	4.76
5	100	10	9.09
6	100	15	13.04

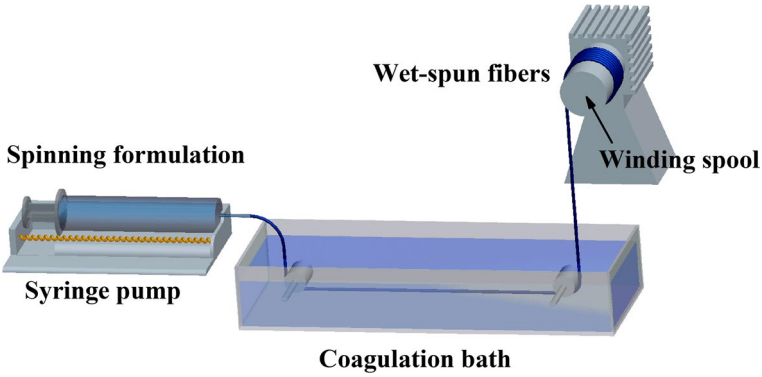

Fig. 1 Schematic of wet-spinning apparatus

schematic of the wet-spinning apparatus used in this study is shown in Fig. 1. Extrusion process was carried out using a syringe pump (KD Scientific) exploring flow rate of 3.6 mL h^{-1}. Composite fibers that came out of coagulation bath were then collected onto a heated winding spool at 60 °C for drying. Linear speed of the winding spool was set at 0.9 m min^{-1}. Thus, six groups of composite fibers with different PEDOT:PSS loadings were successfully prepared. Drying fiber samples were then used for tests and characterizations.

Characterization

Chemical structures and constitutions of composite fiber were characterized using FT-IR spectrometer (Nicolet iS 10, Thermo Fisher Scientific) in the frequency range of 500–4000 cm^{-1}. Surface morphology of composite fiber was observed using scanning electron microscope (SU1510, Hitachi, Japan). Mean value of fiber diameter was calculated using ImageJ analysis software with at least ten points taken on each fiber. Melting behavior and degree of crystallization of composite fiber were measured using differential scanning calorimeter (Q200, TA Instruments, USA). Samples were heated from 30 to 220 °C at a heating rate of 5 °C/min under nitrogen atmosphere. Mechanical stability of composite fibers under dynamic force at rising temperatures was characterized by dynamic mechanical analyzer (Q800, TA Instruments, USA) in the tension mode at a frequency of 1 Hz and in the temperature range from 20 to 150 °C at a heating rate of 3 °C min^{-1}. Thermogravimetric analysis (TGA) and differential thermogravimetric analysis (DTG) were performed using a TGA analyzer (Q500, TA Instruments, USA) in the temperature range of 40–800 °C at a heating rate of 10 °C min^{-1} to evaluate thermal stability of composite fibers. Electrical resistance of composite fiber was measured at room temperature using a high resistance meter (Keithley 6517B, Tektronix Company). Electrodes on fiber were made by connecting a gold thread to fiber surface with silver epoxy. The distance between two contacts was 10 mm. For each sample, ten different segments with same length in a roll of fibers were randomly taken and conductivities were separately measured under same environmental condition. Tensile property of

composite fibers was measured using a tensile testing instrument (EZ-LX, Shimadzu Corporation, Japan) at a constant strain rate of 10% min^{-1}. Samples were fixed on paper cards (20 mm length window) with adhesive tape. Young's modulus, yield stress, tensile strength, and elongation at break were measured with mean value and standard deviations averaged from 10 tests.

Results and discussion

FT-IR spectra analysis

Effect of PEDOT:PSS loading on chemical structure of composite fibers and bonding interaction between PEDOT:PSS and PVA were characterized using FT-IR spectra. Figure 2 shows FT-IR spectra of pure PVA, pure PEDOT:PSS, and PEDOT:PSS/PVA composite fibers with various PEDOT:PSS loadings. In the spectrum of pure PVA, a broad band at 3300 cm^{-1} corresponds to O–H stretching band of hydroxyl group; peak at 2931 cm^{-1} is ascribed to C–H symmetrical stretching vibration. Peaks at 1421, 1327, and 1092 cm^{-1} are assigned to CH–OH bending vibration, C-H in-plane bending vibration, and C–O stretching vibration, respectively [13, 14]. Peaks at 917 and 842 cm^{-1} are related to skeletal stretching vibration of carbon chains [15, 16]. In the spectrum of pure PEDOT:PSS, absorption band at around 2100 cm^{-1} between 2300 and 1900 cm^{-1} is due to the vibration of CO_2 molecules [17–19]. Peak at 1640 cm^{-1} is attributed to stretching vibrations of C=C bonds from aromatic rings of PSS [20]. Peaks at 1495 and 1271 cm^{-1} are assigned to C=C and C–C stretching of quinoid structure originated from thiophene ring [21, 22]. Peaks at 1162 and 1122 cm^{-1} are corresponding to symmetrical vibration of sulfonic acid group in PSS [20, 23]. Peaks at 1063 and 1040 are attributed to C–O–C bond stretching vibration [24]. And peaks at 947, 863, and 715 cm^{-1} are related to C–S bond vibration of thiophene ring in PEDOT [20, 21, 23, 24]. Characteristic peaks

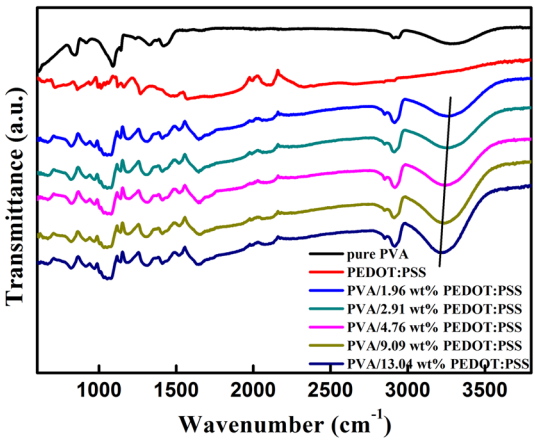

Fig. 2 FT-IR spectra of composite fibers with various PEDOT:PSS loadings

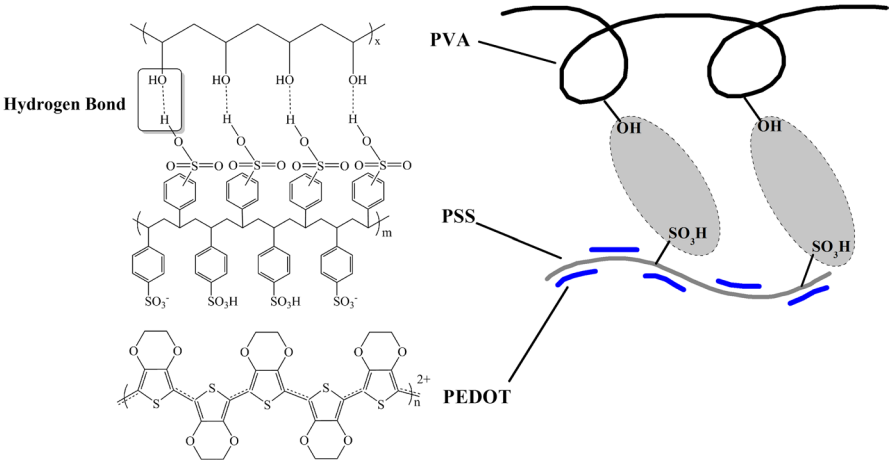

Scheme 1 Schematic of interactions between PVA and PEDOT:PSS in PEDOT:PSS/PVA composite fiber

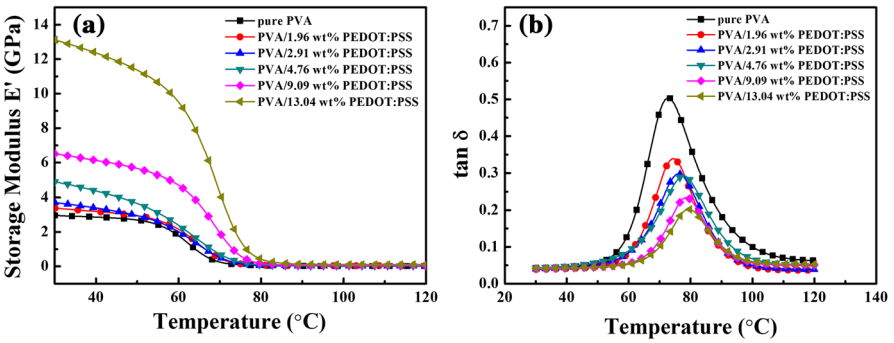

Fig. 3 **a** Storage modulus and **b** tan δ versus temperature curves of PVA/PEDOT:PSS composite fibers at various PEDOT:PSS loadings

of both PVA and PEDOT:PSS are observed from spectra of PVA/PEDOT:PSS composite fibers, indicating successful synthesis of composite fibers. More importantly, it was observed from spectra of composite fibers that the hydroxyl peaks shifted to smaller wave numbers and peak intensity gradually became stronger with increasing PEDOT:PSS loading. This indicated that the hydroxyl groups of PVA interacted with oxygen-containing functional groups ($SO_3^-H^+$) of PEDOT:PSS through hydrogen bonding as illustrated in Scheme 1 [25, 26]. Formation of hydrogen bonding interaction will lead to better miscibility between two components [25] and lead to improvement in fiber properties.

DMA analysis

DMA measurement was carried out to investigate mechanical stability of composite fibers under dynamic force at rising temperatures. Figure 3 shows storage modulus (E') and tan δ of composite fibers at different PEDOT:PSS loadings. It was clearly observed that storage moduli of composite fibers were higher than those of pure PVA fiber. Storage modulus of composite fiber with 1.96 wt% PEDOT:PSS loading was enhanced by around 15% compared to pure PVA fiber. And storage modulus of composite fibers increased with increasing PEDOT:PSS loading. Addition of 13.04 wt% PEDOT:PSS enhanced E' by 344% compared to pure PVA fiber. These observations indicated that addition of PEDOT:PSS significantly reinforced the plasticity of pure PVA. Unlike storage modulus, tan δ_{max} gradually decreased with increasing PEDOT:PSS loading. Decrease in peak value of tan δ was attributed to enhanced stiffness of composite fibers resulted from addition of PEDOT:PSS introducing hard segments into polymer chains of composite fibers. Also, it could be observed from tan δ versus temperature curve that the tan δ peak shifted to higher temperature region with increasing PEDOT:PSS loading, indicating increase in glass transition temperature (T_g) [26, 27]. This was because the chemical bonding interactions between hydroxyl groups of PVA and oxygen-containing functional groups of PEDOT:PSS restricted mobility of macromolecular chains of composite fibers and thus improved the T_g value.

DSC analysis

Effect of PEDOT:PSS loading on thermal property of PEDOT:PSS/PVA composite fiber was characterized by DSC measurement. Figure 4 shows DSC plots of PEDOT:PSS/PVA composite fibers at different PEDOT:PSS loadings. From Fig. 4, glass transition temperature (T_g) of pure PVA fiber was observed at 72.21 °C, which gradually increased and reached 78.83 °C for 13.04 wt% PEDOT:PSS loading. Variation tendency in T_g values was consistent with that in DMA analysis, indicating

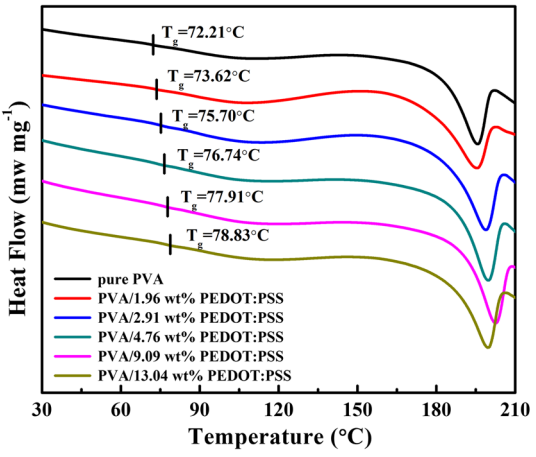

Fig. 4 DSC curves of PEDOT:PSS/PVA composite fibers with various PEDOT:PSS loadings

Table 2 Glass transition temperature (T_g), melting enthalpy (ΔH_m), and crystallinity (χ_c) of PVA/PEDOT:PSS composite fibers at different PEDOT:PSS contents

Sample No.	PEDOT:PSS content (wt %)	T_g (°C)	ΔH_m (J g^{-1})	χ_c (%)
1	0	72.21	58.20	42.00
2	1.96	73.62	59.21	42.72
3	2.91	75.70	62.32	44.96
4	4.76	76.74	63.24	45.62
5	9.09	77.91	61.26	44.20
6	13.04	78.83	61.92	44.68

that PVA chains were stiffened by the hydrogen bonding interactions due to increasing PEDOT:PSS loading [25]. Melting enthalpy (ΔH_m) calculated from area under melting peak and corresponding crystallinity (χ_c) calculated on the basis of the following equation are tabulated in Table 2.

$$\chi_c = \Delta H_m / \Delta H_0, \tag{1}$$

where ΔH_0 is standard melting enthalpy of pure PVA (138.6 J g^{-1}) [28]. From Table 2, no obvious change was observed in crystallinity of composite fibers compared to that of pure PVA fiber, indicating that addition of PEDOT:PSS did not influence crystallinity of PEDOT:PSS/PVA composite fibers.

TGA analysis

Thermal stabilities of composite fibers at different PEDOT:PSS loadings were characterized by TGA analysis. Figure 5 shows thermogravimetric (TGA) and differential thermogravimetric (DTG) plots of composite fibers. It was observed from TGA plots that all composite fibers revealed three weight loss regions. The first region, from 60 to 150 °C, was due to evaporation of bound water; the second region, from 200 to 350 °C, was attributed to degradation of side chains of PVA; the third region,

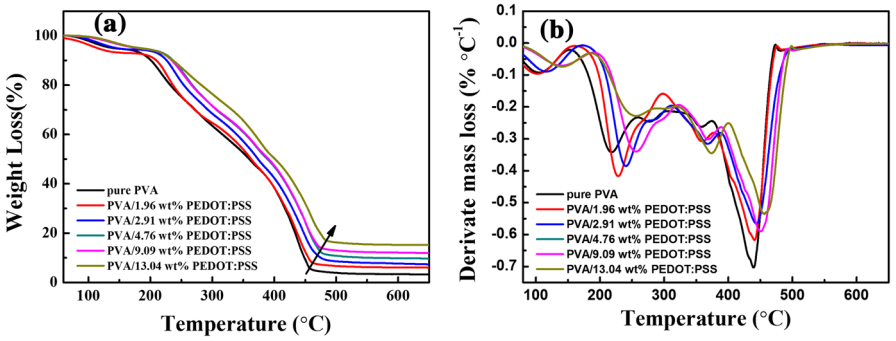

Fig. 5 **a** TGA and **b** DTG plots of PEDOT:PSS/PVA composite fibers with various PEDOT:PSS loadings

from 370 to 470 °C, was caused by decomposition of C–C backbone of PVA [43]. With increase in PEDOT:PSS loading, total weight loss decreased from 96.5% (for pure PVA fiber) to 88.0% (for PVA/PEDOT:PSS composite fiber with 13.04 wt% PEDOT:PSS loading). Degradation peaks of composite fibers became less intense and shifted to higher temperatures as PEDOT:PSS loading increased, indicating that thermal stability of composite fibers was enhanced. From DTG plots, we determined that peak decomposition temperature increased from 438 °C (for pure PVA fiber) to 457 °C (for PVA/PEDOT:PSS composite fiber with 13.04 wt% PEDOT:PSS loading), indicating that hydrogen bonding interactions led to enhancement in intermolecular forces between PEDOT:PSS and PVA, thus enhancing thermal stability of composite fibers. Moreover, area under major degradation peak was measured less for all PEDOT:PSS/PVA composite fibers than that for pure PVA fiber. These observations revealed that increase in PEDOT:PSS loading significantly improved thermal stability of PEDOT:PSS/PVA composite fibers.

Electrical conductivity

Change in conducting filler content will significantly influence electrical conductivity of composite fiber. Therefore, effect of PEDOT:PSS loading on electrical conductivity of PEDOT:PSS/PVA composite fibers was investigated as shown in Fig. 6. It was observed that beginning of conductivity occurred at 2.91 wt% PEDOT:PSS loading, with conductivity of 0.41 S cm^{-1}. Above this loading, conductivity increased monotonically with PEDOT:PSS loading and reached 11.32 S cm^{-1} at 13.04 wt% PEDOT:PSS loading. Changes in electrical conductivity indicated that there existed a minimum content of conducting filler to form a continuous conducting path inside an insulating matrix [29]. When filler loading is below percolation threshold, no conducting path is formed and charge carrier transport cannot be realized [29]. By increasing filler content, distance between filler particles can be reduced and when the distance is below a certain threshold, charge carrier transport will occur via tunneling or hopping between neighboring filler particles [29–31]. Continuously increasing filler content will bring contact between filler particles

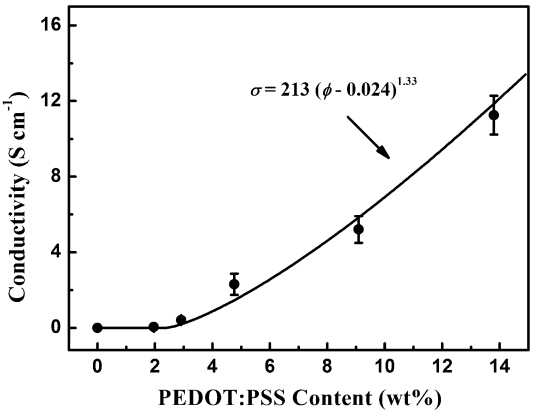

Fig. 6 Electrical conductivity of PEDOT:PSS/PVA composite fibers at different PEDOT:PSS loadings

and therefore create conducting paths, improving conductivity. On the other hand, hydrogen bonding interactions between PVA and PEDOT:PSS are favorable for charge carrier transport due to reducing charge migration barrier [32], thus improving electrical conductivity of composite fiber. In addition, our experimental data fit well with the following equation:

$$\sigma = \sigma_0(\phi - \phi_c)^t, \tag{2}$$

where σ is conductivity of composite fibers; σ_0 is proportionality coefficient; ϕ is volume fraction for each PEDOT:PSS loading; ϕ_c is percolation threshold; and t is critical exponent [30]. We estimated volume fraction (ϕ) for each PEDOT:PSS loading on the basis of assumption that densities of both PVA and PEDOT:PSS are 1.2 g cm^{-3} [33]. According to Eq. 2, a percolation threshold of 2.40 wt% (corresponding to $\phi_c = 0.024$) PEDOT:PSS loading was derived from the fit which is consistent with experimental PEDOT:PSS loading for beginning of conductivity (2.91 wt%) [29]. Valuation method for ϕ_c was referred to Seyedin et al. [29]. The t value was estimated to be 1.33 according to theoretical value for two-dimensional networks [30, 34]. And proportionality coefficient (σ_0) was found to be 213 S cm^{-1} in our case. This value was comparable to conductivity of pure PEDOT:PSS fiber, indicating that PEDOT:PSS conducting filler dispersed homogenously in PVA matrix [29].

Fiber morphology

SEM images of PEDOT:PSS/PVA composite fibers are shown in Fig. 7 to investigate the effect of PEDOT:PSS loading on surface morphology of composite fibers. It was observed that fiber morphology changed from an irregular shape to a regularly circular shape with increasing PEDOT:PSS loading. Composite fiber got a circular shape when PEDOT:PSS loading reached 13.04 wt%. Morphological changes were attributed to difference in mass transfer rate resulted from various spinning

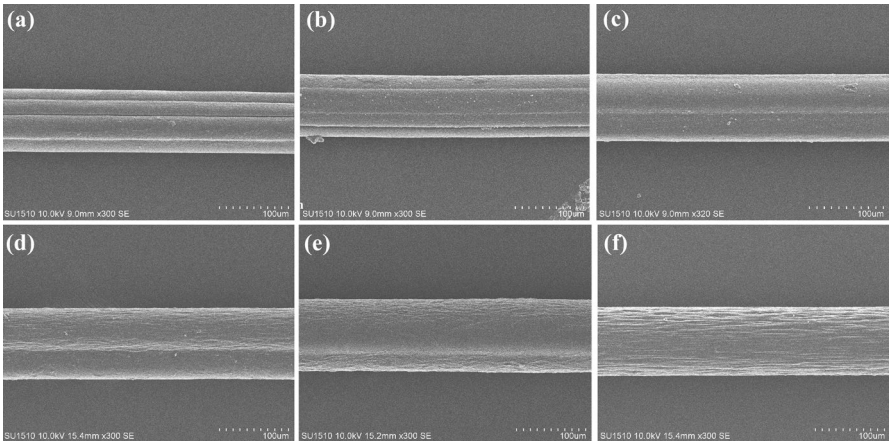

Fig. 7 SEM images of PEDOT:PSS/PVA composite fibers with various PEDOT:PSS loadings

formulation compositions [29, 35]. In wet-spinning process, fibers tend to have irregular shape when the diffusion rate of coagulating solvent (into the spinning formulation) is not equivalent to the extraction rate of spinning formulation (into the coagulation bath) [29]. This process is the so-called mass transfer rate difference. Increase in PEDOT:PSS loading gradually changed mass transfer rate differences and facilitated formation of circular shape of composite fiber. In other words, phase transformation from viscous spinning formulation to solid fiber occurred at different rates for different PEDOT:PSS loadings. In the case of pure PVA wet spinning, fiber formed with solid skin and viscous core. Solid skin tended to collapse into irregular shape when remaining solvent continuously extracted. However, when increased PEDOT:PSS loading in spinning formulation, coagulation rate gradually became slower and facilitated fiber formation with a thinner skin which was favorable for maintaining relative circular shape of fiber.

Tensile property

Tensile test was carried out to investigate the effect of PEDOT:PSS loading on tensile properties of composite fibers, and results are shown in Fig. 8. It was observed that Young's modulus and tensile strength of composite fibers increased with PEDOT:PSS loading, while elongation at break decreased.

Young's modulus of composite fibers increased exponentially with PEDOT:PSS loading from 2.95 GPa (pure PVA fiber) to 12.25 GPa (composite fiber with 13.04 wt% PEDOT:PSS loading). Increase in Young's modulus was due to the addition of PEDOT:PSS, which introduced hard segments into composite fibers. Polymer chain structure of PVA is soft C–C polymer backbones including hydroxyl groups in side chains [36], while polymer backbone of PEDOT:PSS is continuously connected stiff thiophene ring. Addition of PEDOT:PSS introduced hard segments into composite fibers, therefore enhancing Young's modulus of composite fibers, which had also been proved by DMA analysis previously. Experimental value of Young's modulus matched up well with the Mooney's equation [37–41], as shown below:

$$E_c = E_p \times e^{\left(\frac{k_E \phi}{1 - s\phi}\right)}, \tag{3}$$

where E_c is the Young's modulus of composite; ϕ is volume fraction of fillers; E_p is Young's modulus of polymer matrix; k_E is Einstein coefficient; and s represents crowding factor [29, 38]. In our case, the s value was calculated by fitting experimental modulus value with Eq. 3, in which E_p was 2.95 GPa for pure PVA fiber. Fitted s value was found to be 1.70, indicating that PEDOT:PSS filler particles uniformly dispersed within PVA matrix [38]. And k_E has also been calculated to be 7.61 for non-spherical fillers (PEDOT:PSS in our case) which have an aspect ratio of 6.35 [42].

Besides Young's modulus, tensile strength of composite fiber was also observed increased with PEDOT:PSS loading. Addition of PEDOT:PSS induced formation

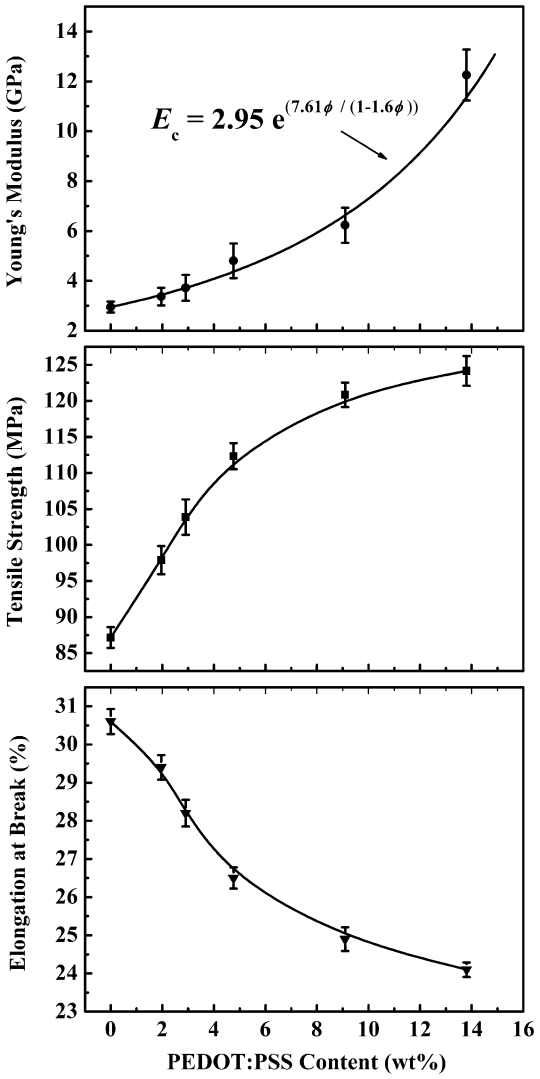

Fig. 8 Tensile properties of PEDOT:PSS/PVA composite fibers with various PEDOT:PSS loadings: **a** Young's modulus, **b** tensile strength, and **c** elongation at break

of hydrogen bonding interactions between oxygen-containing functional groups of PEDOT:PSS and hydroxyl groups of PVA. This interaction enhanced intermolecular forces between two components and led to better miscibility between two components, favorable for reducing structural defects of composite fibers, and finally improved tensile strength of composite fibers. On the other hand, increasing PEDOT:PSS loading facilitated fiber formation with regularly circular shape. This uniform structure can dissipate tensile loadings better than irregular shape, therefore enhancing tensile strength of composite fibers.

Unlike Young's modulus and tensile strength, elongation at break was observed to decrease with PEDOT:PSS loading. Addition of PEDOT:PSS introduced rigid

segments into composite fibers, which disrupted extension of soft segments in PVA at high elongation, and therefore resulted in earlier breakage of composite fibers.

Conclusions

In conclusion, this work systematically investigated the effect of PEDOT:PSS loading on structure and properties of PEDOT:PSS/PVA composite fibers. Addition of PEDOT:PSS induced hydrogen bonding interactions between PEDOT:PSS and PVA, and this interaction was enhanced with increasing PEDOT:PSS loading. Electrical conductivity of composite fibers increased monotonically with PEDOT:PSS loading. The Young's modulus of composite fibers increased with PEDOT:PSS loading due to introduction of hard segments into macromolecular chains. Tensile strength of composite fibers was also improved due to increasing hydrogen bonding interactions between PEDOT:PSS and PVA. Increase in PEDOT:PSS loading also influenced the mass transfer rate difference and therefore facilitated formation of circular shape and smooth surface of composite fibers. Thermal stabilities of composite fibers were also improved as PEDOT:PSS loading increased.

Acknowledgements This work was supported by the National High-tech Research and Development Program of China (No. 2016YFB0302901-3), the Postgraduate Research and Practice Innovation Program of Jiangsu Province (Nos. KYCX17_1142 and KYCX17_1439) and the Postgraduate Research and Innovation Program of Jiangsu Province (Nos. KYCX17_1439, KYCX17_1442).

References

1. Zhou J, Li EQ, Li R, Xu XZ, Ventura IA, Moussawi A et al (2015) Semi-metallic, strong and stretchable wet-spun conjugated polymer microfibers. J Mater Chem C 3(11):2528–2538
2. Ding Y, Invernale MA, Sotzing GA (2010) Conductivity trends of PEDOT-PSS impregnated fabric and the effect of conductivity on electrochromic textile. ACS Appl Mater Interfaces 2(6):1588–1593
3. Jalili R, Razal JM, Innis PC, Wallace GG (2011) One-step wet-spinning process of poly (3, 4-ethylenedioxythiophene): poly (styrenesulfonate) fibers and the origin of higher electrical conductivity. Adv Func Mater 21(17):3363–3370
4. Wang CY, Mottaghitalab V, Too CO, Spinks GM, Wallace GG (2007) Polyaniline and polyaniline–carbon nanotube composite fibres as battery materials in ionic liquid electrolyte. J Power Sources 163(2):1105–1109
5. Coleman JN, Khan U, Gun'ko YK (2006) Mechanical reinforcement of polymers using carbon nanotubes. Adv Mater 19(6):689–706
6. Groenendaal L, Jonas F, Freitag D, Pielartzik H, Reynolds JR (2000) Poly(3, 4-ethylenedioxythiophene) and its derivatives: past, present, and future. Adv Mater 12(7):481–494
7. Trivedi DC, Nalwa HS (1997) Handbook of organic conductive molecules and polymers, vol 2. Wiley, New York, pp 505–572
8. Focke WW, Wnek GE, Wei Y (1987) Influence of oxidation state, pH, and counterion on the conductivity of polyaniline. J Phys Chem 91(22):5813–5818
9. Lux F (1998) Polyaniline auf demPrüfstand. Farbe + Lack 104(8):32
10. Wang Y, Zhu C, Pfattner R, Yan H, Jin L, Chen S et al (2017) A highly stretchable, transparent, and conductive polymer. Sci Adv 3(3):e1602076
11. Choong CL, Shim MB, Lee BS, Jeon S, Ko DS, Kang TH et al (2014) Highly stretchable resistive pressure sensors using a conductive elastomeric composite on a micropyramid array. Adv Mater 26(21):3451–3458

12. Okuzaki H, Harashina Y, Yan H (2009) Highly conductive PEDOT/PSS microfibers fabricated by wet-spinning and dip-treatment in ethylene glycol. Eur Polymer J 45(1):256–261
13. Wang X, Ge MQ, Feng GY (2015) The effects of DMSO on structure and properties of PVA/PEDOT:PSS blended fiber. Fibers Polym 16(12):2578–2585
14. Wang X, Feng GY, Ge MQ (2017) Influence of ethylene glycol vapor annealing on structure and property of wet-spun PVA/PEDOT:PSS blend fiber. J Mater Sci 52(12):6917–6927
15. Pandey M, Joshi GM, Deshmukh K, Ghosh NN, Raj NAN (2015) Electrical conductivity, optical properties and mechanical stability of 3, 4, 9, 10-perylenetetracarboxylic dianhidride based organic semiconductor. J Phys Chem Solids 80:52–61
16. Patra N, Martinová L, Stuchlik M, Černík M (2015) Structure–property relationships in Sterculiaurens/polyvinyl alcohol electrospun composite nanofibres. Carbohyd Polym 120:69–73
17. Xu S, Liu C, Xiao Z, Zhong W, Luo Y, Ou H et al (2017) Cooperative effect of carbon black and dimethyl sulfoxide on PEDOT:PSS hole transport layer for inverted planar perovskite solar cells. Sol Energy 157:125–132
18. Lei Y, Oohata H, Kuroda SI, Sasaki S, Yamamoto T (2005) Highly electrically conductive poly (3, 4-ethylenedioxythiophene) prepared via high-concentration emulsion polymerization. Synth Met 149(2):211–217
19. Ely F, Matsumoto A, Zoetebier B, Peressinotto VS, Hirata MK, de Sousa DA et al (2014) Handheld and automated ultrasonic spray deposition of conductive PEDOT:PSS films and their application in AC EL devices. Org Electron 15(5):1062–1070
20. Stefanescu EA, Tan X, Lin Z, Bowler N, Kessler MR (2011) Multifunctional fiberglass-reinforced PMMA-$BaTiO_3$ structural/dielectric composites. Polymer 52(9):2016–2024
21. Zhou H, Han G, Chang Y, Fu D, Xiao Y (2015) Highly stable multi-wall carbon nanotubes@ poly (3, 4-ethylenedioxythiophene)/poly (styrene sulfonate) core–shell composites with three-dimensional porous nano-network for electrochemical capacitors. J Power Sources 274:229–236
22. Balamurugan A, Ho KC, Chen SM (2009) One-pot synthesis of highly stable silver nanoparticles-conducting polymer nanocomposite and its catalytic application. Synth Met 159(23):2544–2549
23. Xu Y, Wang Y, Liang J, Huang Y, Ma Y, Wan X et al (2009) A hybrid material of graphene and poly (3, 4-ethyldioxythiophene) with high conductivity, flexibility, and Transparency. Nano Res 2:343–348
24. Zhang H, Xu J, Wen Y, Wang Z, Zhang J, Ding W (2015) Conducting poly (3, 4-ethylenedioxythiophene): poly (styrene-sulfonate) film electrode with superior long-term electrode stability in water and synergistically enhanced electrocatalytic ability for application in electrochemical sensors. Synth Met 204:39–47
25. Lee JH, Jung JP, Jang E, Lee KB, Hwang YJ, Min BK et al (2016) PEDOT-PSS embedded comb copolymer membranes with improved CO_2 capture. J Membr Sci 518:21–30
26. Yu DS, Kuila T, Kim NH, Lee JH (2014) Enhanced properties of aryl diazonium salt-functionalized graphene/poly (vinyl alcohol) composites. Chem Eng J 245:311–322
27. Yang CC, Chien WC, Li YJ (2010) Direct methanol fuel cell based on poly (vinyl alcohol)/titanium oxide nanotubes/poly (styrene sulfonic acid)(PVA/nt-TiO 2/PSSA) composite polymer membrane. J Power Sources 195(11):3407–3415
28. Shen B, Zhai W, Lu D, Wang J, Zheng W (2012) Ultrasonication-assisted direct functionalization of graphene with macromolecules. RSC Adv 2(11):4713–4719
29. Seyedin MZ, Razal JM, Innis PC, Wallace GG (2014) Strain-responsive polyurethane/PEDOT:PSS elastomeric composite fibers with high electrical conductivity. Adv Func Mater 24(20):2957–2966
30. Stauffer D, Aharony A (1994) Introduction to percolation theory. CRC Press, Boca Raton
31. StruMpler R, Glatz-Reichenbach J (1999) Feature article conducting polymer composites. J Electroceram 3(4):329–346
32. Akiba I, Masunaga H, Sasaki K, Shikasho K, Sakurai K (2004) Nanostructured polymer blend formed from poly (N-vinylpyrrolidone) and end-functional polystyrene. Polymer 45(17):5761–5764
33. Jalili R, Razal JM, Wallace GG (2012) Exploiting high quality PEDOT:PSS–SWNT composite formulations for wet-spinning multifunctional fibers. J Mater Chem 22(48):25174–25182
34. Bauhofer W, Kovacs JZ (2009) A review and analysis of electrical percolation in carbon nanotube polymer composites. Compos Sci Technol 69(10):1486–1498
35. Mishra SP (2000) A text book of fibre science and technology. New Age International, New Delhi
36. Gaur SS, Dhar P, Sonowal A, Sharma A, Kumar A, Katiyar V (2017) Thermo-mechanically stable sustainable polymer based solid electrolyte membranes for direct methanol fuel cell applications. J Membr Sci 526(5):348–354

37. Mooney M (1951) The viscosity of a concentrated suspension of spherical particles. J Colloid Sci 6(2):162–170
38. Lewis TB, Nielsen LE (1970) Dynamic mechanical properties of particulate-filled composites. J Appl Polym Sci 14(6):1449–1471
39. Ahmed S, Jones FR (1990) A review of particulate reinforcement theories for polymer composites. J Mater Sci 25(12):4933–4942
40. Rao Y, Pochan JM (2007) Mechanics of polymer − clay nanocomposites. Macromolecules 40(2):290–296
41. Fu SY, Feng XQ, Lauke B, Mai YW (2008) Effects of particle size, particle/matrix interface adhesion and particle loading on mechanical properties of particulate–polymer composites. Compos B Eng 39(6):933–961
42. Brodnyan JG (1959) The concentration dependence of the Newtonian viscosity of prolate ellipsoids. Trans Soc Rheol 3(1):61–68
43. Torabi B, Ameri E (2016) Methyl acetate production by coupled esterification-reaction process using synthesized cross-linked PVA/silica nanocomposite membranes. Chem Eng J 288:461–472